

Radiation Signatures of Electron Acceleration in the Decelerating Jet of MAXI J1348-630

AISHWARYA SARATH¹ AND MARKUS BÖTTCHER ²

¹*St Joseph's University
Langford Road , Bangalore
Karnataka,India*

²*Center for Space Research
North-West University
Potchefstroom, South Africa*

ABSTRACT

A discrete jet component (blob) ejection and its subsequent deceleration were observed in the 2019/2020 outburst of the low-mass X-ray binary MAXI J1348-630. A first kinematic analysis of the deceleration due to an abrupt transition from an evacuated cavity to the interstellar medium suggested a kinetic energy exceeding 10^{46} erg, surpassing estimates of the available total ejection energy. However, incorporating a transition layer with exponential density growth between the cavity and the interstellar medium recently enabled a kinematic analysis with much more realistic energy requirements of approximately 10^{44} erg. Here, we study the expected radiative signatures of electrons accelerated within the decelerating blob by introducing a model akin to the relativistic blast wave model for gamma-ray bursts, considering radiative energy losses and radiation drag, to simulate the deceleration of a relativistically moving plasmoid. This model yields snap-shot spectral energy distributions and multi-wavelength light curves from synchrotron and synchro-self-compton (SSC) emission. Notably, the synchrotron emission peaks in the X-rays, but the predicted X-ray flux is negligible compared to thermal emission from the accretion disk. The predicted radio light curve closely resembles the observed one during the jet deceleration phase following the outburst in 2019/2020.

Keywords: Astrophysical jets (33) ; X-ray binaries (1907)

1. INTRODUCTION

MAXI J1348-630 is classified as a black-hole low-mass X-ray binary (BH LMXB) system, where a low-mass companion star fills its Roche lobe, feeding a hot accretion disk surrounding the compact object. In a subset of X-ray binary systems, including MAXI J1348-630, a fraction of the accreted matter is channeled into mildly relativistic jets, in which case they are termed microquasars. They are regarded as scaled-down counterparts of radio-loud active galactic nuclei (AGNs), sharing many of the same features. This resemblance provides a valuable opportunity to study the scale-invariant properties of black holes, especially those related to the interplay between accretion and ejection, as these processes evolve through various regimes and timescales (Körding & Falcke 2005; Carotenuto et al. 2021; Sanna et al. 2022).

An effective approach for identifying X-Ray Binaries (XRBs) and studying their state changes involves continuous X-ray monitoring of the entire sky. This is particularly useful because most XRBs are transient sources and display unpredictable X-ray outbursts (e.g., Tominaga et al. 2020; Corbel et al. 2000a; Hannikainen et al. 1998; Markoff et al. 2003). The MAXI (Monitor of the All-Sky X-Ray Image) instrument, mounted on the International Space Station, scans about 85 % of the sky every 92 minutes (Matsuoka et al. 2009; Koljonen & Russell 2019). It captures each section of the sky for 40 – 100 seconds during each orbit. MAXI is specifically designed for detecting and studying black hole X-ray binary systems. Since 2009, MAXI has found 13 new XRBs and regularly observed their state changes.

Synchrotron emission from compact jets is responsible for the radio to infrared emission observed in black-hole X-ray binaries (BHXRBs; Fender 2003; Kajava et al. 2019). Black hole transients remain in a quiescent state for extended periods, often lasting several months to years or even decades. During their outbursts, they emit radiation across a wide range of wavelengths, from radio waves to X-rays (e.g., Carotenuto et al. 2021). During an outburst, the

system transitions through various accretion states, each with distinct spectral and timing characteristics (Remillard & McClintock 2006; Belloni 2010; Bambi 2016). Initially, it exhibits a rising hard X-ray state dominated by non-thermal power-law emission due to inverse-Compton scattering by hot electrons near the compact object. As the accretion rate increases, the system moves into an intermediate state where the X-ray spectrum softens due to increased thermal emission from the accretion disk (Corbel et al. 2003; Homan et al. 2013; Chen & Podsiadlowski 2019; Markoff et al. 2003). Eventually, it reaches the soft state, characterized by dominant thermal emission from an optically thick, geometrically thin accretion disk truncating at the innermost stable circular orbit (ISCO). Later, the system returns to a hard state before slowly approaching quiescence (Ingram & Motta 2019; Zdziarski & Gierliński 2004; Poutanen et al. 2014; Steiner et al. 2010).

Some BH LMXBs launch transient jets, which are relativistic plasma blobs ejected in opposite directions (Mirabel & Rodríguez 1994; Hjellming & Rupen 1995). During outbursts, the jets of BH LMXBs evolve significantly. In the hard state, compact jets emit self-absorbed synchrotron radiation, resulting in a flat or slightly inverted radio spectrum (Corbel et al. 2000b; Fender 2001). These jets can contribute to hard X-ray emission and may accelerate matter to relativistic bulk Lorentz factors of a few (Markoff et al. 2005; Ribo et al. 2004). In the soft state, the jets are quenched, with a significant drop in radio emission (Fender et al. 1999; Corbel et al. 2000b). When transitioning back to the hard state, jets are gradually reactivated (Miller-Jones et al. 2012; Kalemci et al. 2013). These jets can display apparent superluminal motion and emit optically thin radio waves as they interact with the interstellar medium (Corbel et al. 2002a; Tomsick et al. 2003a). Although transient jets are associated with strong radio flares near state transitions, the exact jet-launching mechanism remains unclear (Fender et al. 2004; Corbel et al. 2004).

MAXI J1348-630 was discovered by the MAXI detector during a giant outburst on 2019 January 26 (MJD 58,509, Yatabe et al. 2019). Using MeerKAT and Australia Telescope Compact Array (ATCA) observations, Carotenuto et al. (2021) observed the ejection of compact radio jet components associated with the major X-ray outburst at speeds $\geq 0.69 c$, and their subsequent deceleration. Different estimates of the distance to the source exist: approximately $2.2_{-0.6}^{+0.5}$ kpc using H I absorption (Chauhan et al. 2020), and about 3.4 ± 0.3 kpc based on X-ray observations of a dust-scattering halo (Lamer et al. 2021). In this work, we use the value of $D = 2.2$ kpc.

The *Neil Gehrels Swift* X-Ray Telescope (XRT) monitored the source with 85 pointings over a period of almost 1 year, beginning shortly after the discovery of the outburst on January 26, 2019 (see Carotenuto et al. 2021, for more information on the observations and data reduction). As discussed in Carotenuto et al. (2021), the outburst began with a rapid increase in X-ray brightness, which was first detected on MJD 58509. Initially, the system was in the hard state, characterized by a power-law X-ray spectrum indicative of emission from a hot corona. As the outburst progressed, the X-ray emission became softer, transitioning through different states: from the hard state to the intermediate state (IMS) on February 3, 2019 (MJD 58517), and then to the soft state on February 8, 2019 (MJD 58522.6). During the soft state, the X-ray spectrum was dominated by thermal emission from the accretion disk, with a peak disk temperature of around 0.8 keV. The system remained in the soft state as it reached peak flux of the outburst and then began a gradual decay. After about two months, the system transitioned back to the IMS on March 26, 2019 (MJD 58597), and eventually returned to the hard state on April 2, 2019 (MJD 58604). The optical counterpart of MAXI J1348-630 was discovered on 2019 January 26 using the iTelescope.Net T31 instrument in Siding Spring, Australia. A new optical transient at R.A. = 13h48m12.88s, Decl. = $-63^{\circ}16'28.4''$ (J2000.0) with a magnitude of 16.18 was identified within the Swift error circle, 82 arcseconds from its center. (Denisenko et al. 2019; Kennea & Negoro 2019; Nesci & Focci 2019; Russell et al. 2019a)

The initial, major outburst was followed by three smaller flares over the course of the next few months, labelled R1 – R3, in accordance with the nomenclature of Carotenuto et al. (2021). The slow decay of the X-ray light curve during the initial outburst is well described by disk-dominated emission. As described in Carotenuto et al. (2021), during this phase, the strong jets might have cleared out or displaced the surrounding ISM, creating a low-density cavity around the black hole system. The presence of this cavity is the basis for the cavity – ISM transition models of Carotenuto et al. (2022) and Zdziarski et al. (2023) for the radio-jet deceleration.

The deceleration of the compact jet components ejected by MAXI J1348-630 in tandem with the radio flare RK1, was modelled by Carotenuto et al. (2022), assuming a sharp transition from an evacuated cavity to the interstellar medium (ISM). Their kinematic analysis required the ejecta to have an initial energy of $E_0 = 4.6_{-3.4}^{+20} \times 10^{46} (\phi/1^{\circ})(n_{\text{ISM}}/(1 \text{ cm}^{-3}))$ erg, where ϕ is the opening angle of the jet and n_{ISM} the particle density of the ISM. This energy is significantly beyond the limit corresponding to magnetically arrested accretion onto a maximally rotating stellar-mass black hole. As a sharp transition from an evacuated cavity to the ISM is likely not a realistic assumption,

Zdziarski et al. (2023) introduced an extension of the model of Carotenuto et al. (2022), considering a transition layer between the cavity and the ISM with exponential density growth. The kinematic analysis using such a density profile resulted in a much more realistic kinetic energy value of about $\sim 10^{44}$ erg.

In this paper, we study the multi-wavelength radiative signatures expected from the acceleration of particles at the shock front formed by the interaction of the ejected plasmoid ('blob') with the surrounding medium. We describe our analysis of the kinematics of the decelerated blob, the resulting relativistic electron distribution, and the evaluation of snap-shot SEDs and radio light curve fits in §2. Numerical results are presented and compared to observations in §3. We summarize and discuss our results in §4.

2. MODEL OF A DECELERATING JET

Following Zdziarski et al. (2023), we assume a thin transition layer between the evacuated cavity (with density $n_{\text{cavity}} \ll 1 \text{ cm}^{-3}$) and the ISM with standard density $n_{\text{ISM}} = 1 \text{ cm}^{-3}$. The inner boundary of the transition layer is at a distance r_c from the black hole, from where the density begins to grow exponentially with an e-folding distance dr until it reaches the density of the ISM at r_{ISM} :

$$n(r) = \begin{cases} n_{\text{cavity}} & \text{if } r \leq r_c, \\ n_{\text{cavity}} e^{(r-r_c)/d_r} & \text{if } r_c \leq r \leq r_{\text{ISM}}, \\ n_{\text{ISM}} & \text{if } r \geq r_{\text{ISM}}. \end{cases} \quad (1)$$

$$r_{\text{ISM}} = r_c + d_r \ln q, \quad q = \frac{n_{\text{ISM}}}{n_{\text{cavity}}} \quad (2)$$

In the next section we will discuss the kinematics of a mildly relativistic plasmoid interacting with an external medium with the above density profile.

2.1. Jet kinematics

To model the kinematics of a decelerating blob using a momentum-conservation approach, we use the methods of Böttcher & Principe (2009), which were developed to model a quasi-exponential light-curve decay observed in the blazar 3C279. We here develop a scaled-down version of that model appropriate for the scales of microquasars. The work of Böttcher & Principe (2009), in turn, was based on an adaptation of the blast wave model for GRB afterglows (e.g. Chiang & Dermer 1999) to blazar jets. A plasmoid moving with initial mass M_0 and initial bulk Lorentz factor Γ_0 moves along the jet. As it moves, it sweeps up mass from the external medium, thus increasing its mass M . The total momentum P of the plasmoid in the stationary frame is $P = \beta \Gamma M c$ and is conserved, except for momentum imparted on anisotropically emitted radiation. If the plasmoid emits energy evenly in all directions in its rest frame, as is commonly assumed for synchrotron and synchrotron-self-Compton (SSC) emission, its momentum remains constant over time, $dP/dt = 0$. However, if a significant amount of particle energy is lost to Compton scattering of an external radiation field (EC = External Compton), the momentum in this EC flux is lost to the plasmoid. Hence, the equation governing the rate of change of momentum, (dP/dt) , can be expressed as (Böttcher & Principe 2009)

$$\frac{dP}{dt} = \left(\frac{dP}{dt} \right)_{\text{EC}} = \frac{cM\dot{\Gamma}}{\beta} + \Gamma\beta\dot{M}c. \quad (3)$$

Although in the specific model setup for MAXI J1348-630, EC radiation is negligible compared to synchrotron and SSC emission, our code does account for EC energy and momentum losses, using Eqs. (3) and (4) in Böttcher & Principe (2009), in order to keep the model more generally applicable.

Relativistic mass-energy in the plasmoid is not only gained by sweeping up external material, but also lost through radiative dissipation. Hence, the change in relativistic mass may be expressed as

$$\dot{M} = A(r)\rho(r)\Gamma(r)\frac{dr}{dt} + \frac{1}{c^2}\dot{E}_{\text{rad}}, \quad (4)$$

The radial velocity dr/dt is given by βc with $\beta = \sqrt{1 - 1/\Gamma^2}$. The cross-section of the jet $A(r)$ is given by $\pi R_b^2(r)$ with $R_b(r)$ being the radius of the jet. $\rho(r)$ represents the density of the external material being swept up by the plasmoid. The radiative energy loss is given by

$$\dot{E}_{\text{rad}} = -\frac{1}{\Gamma} \frac{4}{3} c \sigma_T u \int_{\gamma_{\min}}^{\gamma_{\max}} N_e(\gamma) \gamma^2 d\gamma \quad (5)$$

where u is the sum of the energy densities in the magnetic and radiation fields ($u_B + u_{\text{ext}} + u_{\text{sy}}$), and we assume that Compton scattering is occurring predominantly in the Thomson regime.

Derivatives with respect to time can be converted into derivatives with respect to the distance r from the central engine using the radial velocity above. This leaves us with the set of coupled differential equations for $\Gamma(r)$, $M(r)$, and $\beta(r)$:

$$\frac{d\Gamma}{dr} = -\Gamma(r)\beta^2(r) \frac{dM/dr}{M(r)} + \frac{\Gamma^2 \dot{E}_{\text{EC}}}{4\pi M c^3} \quad (6)$$

$$\frac{dM}{dr} = A(r)\rho(r)\Gamma(r) + \frac{\dot{E}_{\text{rad}}}{\Gamma(r)\beta(r)c^3} \quad (7)$$

$$\frac{d\beta}{dr} = \frac{d\Gamma}{dr} \frac{1}{\beta\Gamma^3} \quad (8)$$

As in [Böttcher & Principe \(2009\)](#), the radiating relativistic electron energy distributions is obtained assuming a continuous injection of relativistic particles instantaneously accelerated into a power-law spectrum, described by an injection function $Q(\gamma) = Q_0 \gamma^{-q} H(\gamma_{\min}, \gamma, \gamma_{\max})$. The low-energy cutoff, γ_{\min} , is determined by the fraction of swept-up power transferred to relativistic electrons, while the high-energy cutoff, γ_{\max} , is set by balancing the acceleration timescale with the synchrotron loss timescale. The critical electron energy, γ_c , is the energy beyond which particles radiate away energy faster than they can escape, leading to a broken power law distribution depending on whether the cooling is slow or fast. In the slow-cooling regime, $\gamma_c > \gamma_{\min}$, and in the fast-cooling regime, $\gamma_c < \gamma_{\min}$. This results in the broken power-law distributions as used in [Böttcher & Principe \(2009\)](#), depending on whether the system is in the slow-cooling or the fast-cooling regime:

$$N_e(\gamma) = N_0 \begin{cases} \left(\frac{\gamma}{\gamma_b}\right)^{-p_1} & \text{if } \gamma_1 < \gamma < \gamma_b \\ \left(\frac{\gamma}{\gamma_b}\right)^{-p_2} & \text{if } \gamma_b < \gamma < \gamma_2 \end{cases} \quad (9)$$

Here, N_0 is the normalization constant. In the slow cooling regime, the parameters γ_1 , γ_b , and γ_2 correspond to γ_{\min} , γ_c , and γ_{\max} , respectively. The indices p_1 and p_2 correspond to q and $q+1$. In the fast cooling regime the parameters γ_1 , γ_b , and γ_2 correspond to γ_c , γ_{\min} , and γ_{\max} , respectively. The indices p_1 and p_2 correspond to 2 and $q+1$. In the case of MAXI J1348-630, we find that the electron energy distribution is always in the slow cooling regime.

2.2. Analytic solutions to the equation of motion

Eqs. 6 and 7 constitute the equations of motion derived from momentum conservation. If the jet is conical, then $A(r) = \Omega_j r^2$, where Ω_j is the solid angle subtended by the jet; if it is cylindrical, then $A(r) \equiv A_0$. Analytical solutions to the coupled differential equations 6 and 7 may be found in the limiting case where the swept-up mass M_{sw} is negligibly small compared to the initial mass M_0 , i.e., $M_0 \gg M_{\text{sw}}$, and the radiative energy and momentum loss terms are negligible, hence keeping only the first terms on the r.h.s. of Eqs. 6 and 7. The former condition limits the applicability of the solution to the early slowdown phase, either with $\rho(r) = \rho_c$ for $r \leq z_c$ or $\rho(r) = \rho_c e^{(r-z_c)/dz}$ for $z_c \leq r \leq z_c + dz$.

2.2.1. Motion inside the cavity

Inside the cavity ($r < z_c$), the equation of motion for $\Gamma(r)$ for the conical-jet case reduces to

$$\frac{d\Gamma(r)}{dr} \approx -\frac{\Gamma^2(r)\beta^2(r)\Omega_j\rho_c}{M_0} r^2 = -\frac{(\Gamma^2(r)-1)\Omega_j\rho_c}{M_0} r^2 \quad (10)$$

Separation of variables and integration yields an analytical solution of the form

$$\ln\left(\frac{\Gamma(r)+1}{\Gamma(r)-1}\right) - \ln\left(\frac{\Gamma_0+1}{\Gamma_0-1}\right) = \frac{2}{3}\Omega_j\rho_c \frac{r^3-r_0^3}{M_0} \equiv B_{\text{con}}(r) \quad (11)$$

In the case of a cylindrical jet, the solution for $r < z_c$ simplifies to

$$\ln\left(\frac{\Gamma(r)+1}{\Gamma(r)-1}\right) - \ln\left(\frac{\Gamma_0+1}{\Gamma_0-1}\right) = \frac{2A_0\rho_c}{M_0}(r-r_0) \equiv B_{\text{cyl}}(r). \quad (12)$$

Defining,

$$C_{\text{con/cyl}}(r) \equiv \frac{\Gamma_0+1}{\Gamma_0-1} e^{B_{\text{con/cyl}}(r)} \quad (13)$$

one finds the final analytical solution as

$$\Gamma(r) = \frac{C_{\text{con/cyl}}(r)+1}{C_{\text{con/syl}}(r)-1} \quad (14)$$

One easily verifies that for $r = r_0$, $\Gamma(r) = \Gamma_0$ and for $r \rightarrow \infty$, $\Gamma(r) \rightarrow 1$, as expected.

2.2.2. Motion inside the transition zone

In the transition zone ($z_c < r < z_c + dz$) Eq. 6 for a conical jet reduces to

$$\frac{d\Gamma(r)}{dr} \approx -\frac{(\Gamma^2(r)-1)\Omega_j\rho_c e^{-\frac{z_c}{dz}} r^2 e^{\frac{r}{dz}}}{M_0} \quad (15)$$

Again, separation of variables and integration yields with $\Gamma_c = \Gamma(r_c)$.

$$\ln\left(\frac{\Gamma(r)+1}{\Gamma(r)-1}\right) - \ln\left(\frac{\Gamma_c+1}{\Gamma_c-1}\right) = \frac{2\Omega_j\rho_c e^{-\frac{z_c}{dz}}}{M_0} \left(\frac{r^3 e^{\frac{r}{dz}}}{3} - \frac{r_c^3 e^{\frac{r_c}{dz}}}{3}\right). \quad (16)$$

In the case of a cylindrical jet, we have

$$\frac{d\Gamma(r)}{dr} \approx -\frac{(\Gamma^2(r)-1)A_0\rho_c e^{-\frac{z_c}{dz}} e^{\frac{r}{dz}}}{M_0} \quad (17)$$

with the solution

$$\ln\left(\frac{\Gamma(r)+1}{\Gamma(r)-1}\right) - \ln\left(\frac{\Gamma_c+1}{\Gamma_c-1}\right) = \frac{2A_0\rho_c e^{-\frac{z_c}{dz}}}{M_0} \left(e^{\frac{r}{dz}} - e^{\frac{r_c}{dz}}\right) dz \quad (18)$$

These equations may be solved for $\Gamma(r)$ analogous to Eq. 14. One again easily sees that $\Gamma(r_c) = \Gamma_c$ and $\Gamma(r \rightarrow \infty) \rightarrow 1$.

For our numerical modeling of MAXI J1348-63, we considered a cylindrical jet shape. Fig. 1 shows the comparison between the full numerical solutions for $\Gamma(r)$ and $\beta(r)$ and these analytical approximations. The figure illustrates that the agreement is good while the blob is still inside the cavity and entering the transition zone, but as more and more mass is swept up and radiative energy losses become substantial, the approximations break down, as expected. Therefore, for the purpose of our numerical study of the radiative signatures of this model, we used the full numerical solutions. Yet, this comparison to analytical solutions instills confidence that our numerical solutions describe the deceleration process accurately.

2.3. Radiative Output

We used the **JetSet** (Tramacere et al. 2009, 2011; Tramacere 2020) software to calculate the synchrotron and synchrotron self-Compton (SSC) spectral energy distributions (SEDs). The computation of the synchrotron SED in **JetSet** follows the approach outlined by Dermer & Menon (2010) and Finke et al. (2008) which utilize the approximation provided by Aharonian et al. (2010) for the pitch-angle-averaged synchrotron power, which simplifies the integration over the time-evolving electron distribution.

For the SSC SED, **JetSet** again follows the methodologies described by Dermer & Menon (2010) and Finke et al. (2008). The SSC process involves the scattering of synchrotron photons by the same electrons that emitted them. The Compton scattering kernel used (Jones 1968) accounts for the kinematic constraints and cross section for Compton scattering in both the Thomson and Klein-Nishina regimes.

We can estimate the external radiation energy density due to direct accretion-disk photons as $u_{\text{ext}} \sim L_d/(4\pi r^2) \sim 10^{-16} \text{erg cm}^{-3}$ which is much smaller than the magnetic-field energy density, $u_B \sim 10^{-7} \text{erg cm}^{-3}$. To our knowledge, no measurement of the IR - optical - UV emission from the putative companion star exists in the literature, suggesting that the corresponding radiation energy density is also negligible. Therefore, we have omitted EC radiation.

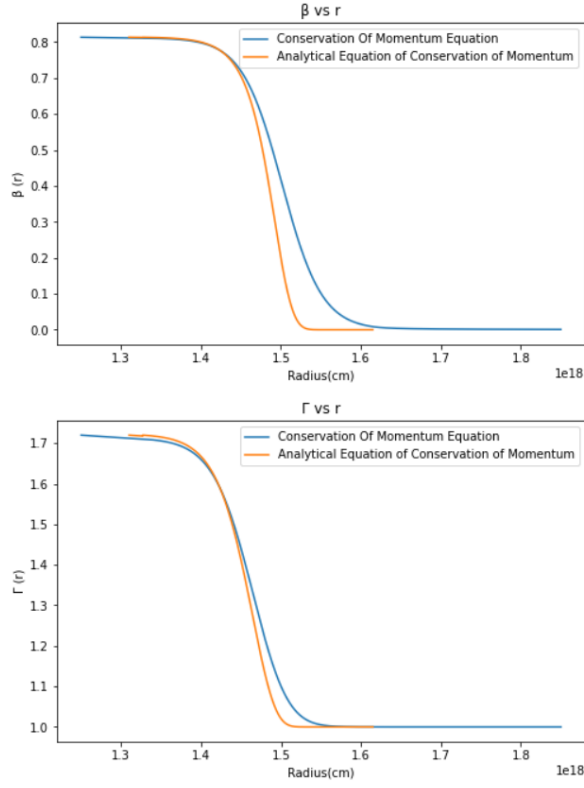


Figure 1. Comparison of the analytical and numerical solutions to the plasmoid deceleration process in a cylindrical jet.

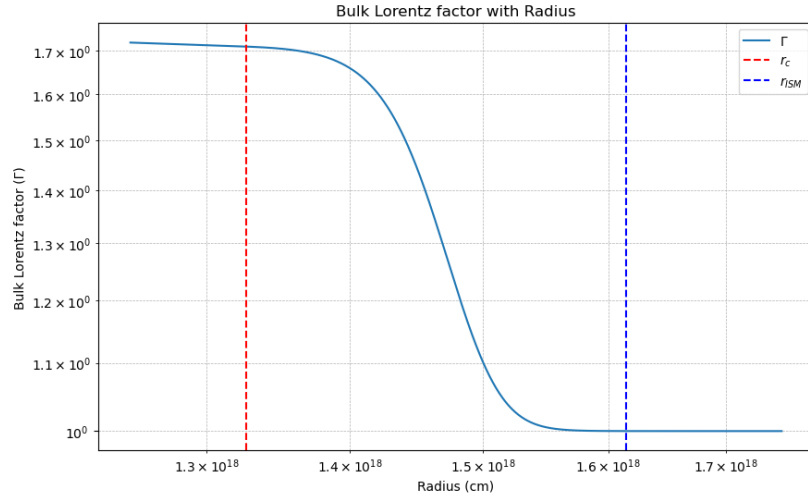
Parameter	Symbol	Value
Initial Lorentz Factor	Γ_0	1.70
Initial Mass	M_0	4.3×10^{23} g
Plasmoid Radius	R_b	2.3×10^{16} cm
Relativistic Electron Fraction	ξ_e	0.5
Transition Region	r_c	1.327×10^{18} cm
Interstellar Medium Density	n_{ISM}	1 cm^{-3}
Cavity Density	n_{Cavity}	10^{-5} cm^{-3}
Magnetic Field Strength	B	0.0043 G
Electron Injection Index	q	2.5
efolding distance	d_r	2.5×10^{16} cm

Table 1. Parameters for the plasmoid evolution model for MAXI J1348-630

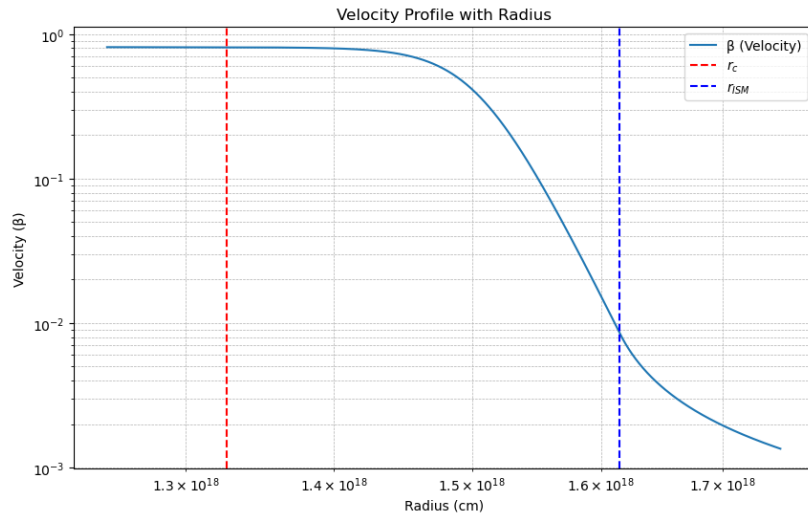
3. NUMERICAL RESULTS: SPECTRAL ENERGY DISTRIBUTIONS (SEDS) AND MULTI-WAVELENGTH LIGHT CURVES

The decelerating-blob model outlined above was applied specifically to the observed plasmoid deceleration of the radio jet component RK1 in MAXI J1348-630 in 2020. The jet geometry was assumed to be cylindrical. The density profile (Eq. 1), initial bulk Lorentz factor, and other parameters, as listed in Table 1, are taken or derived from Zdziarski et al. (2023). The jet viewing angle θ was kept at 30° .

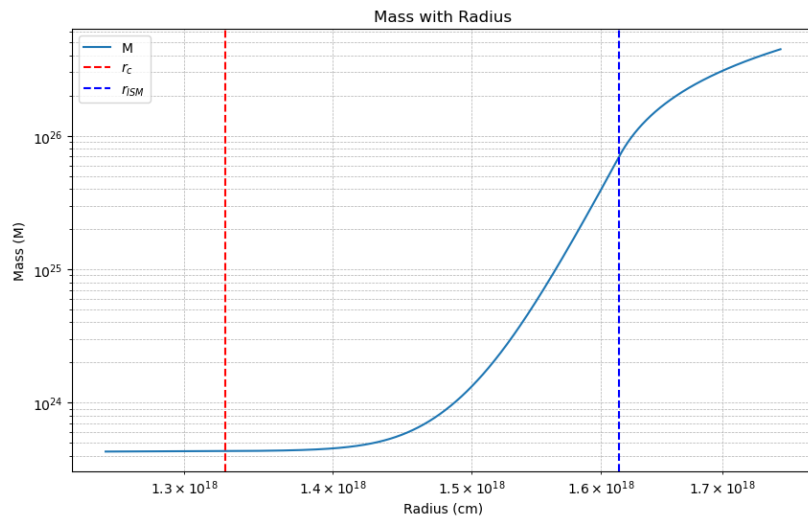
Figure 2 illustrates the evolution of the bulk Lorentz factor Γ , the normalized velocity β , and total mass of the plasmoid with distance, obtained by numerically solving the coupled set of equations 6, 7, and 8. As the plasmoid approaches the transition to the ISM, the bulk Lorentz factor levels off at 1, while the the dimensionless velocity continues to decrease. As in the case of GRBs, we see that the plasmoid evolves through a coasting phase where the bulk Lorentz factor remains approximately constant at Γ_0 and begins to decelerate around the charecteristic



(a)



(b)



(c)

Figure 2. (a) Bulk Lorentz factor Γ . (b) Dimensionless velocity β . (c) Total mass of the plasmoid M . The dashed vertical lines indicate r_c (red) and r_{ISM} (blue).

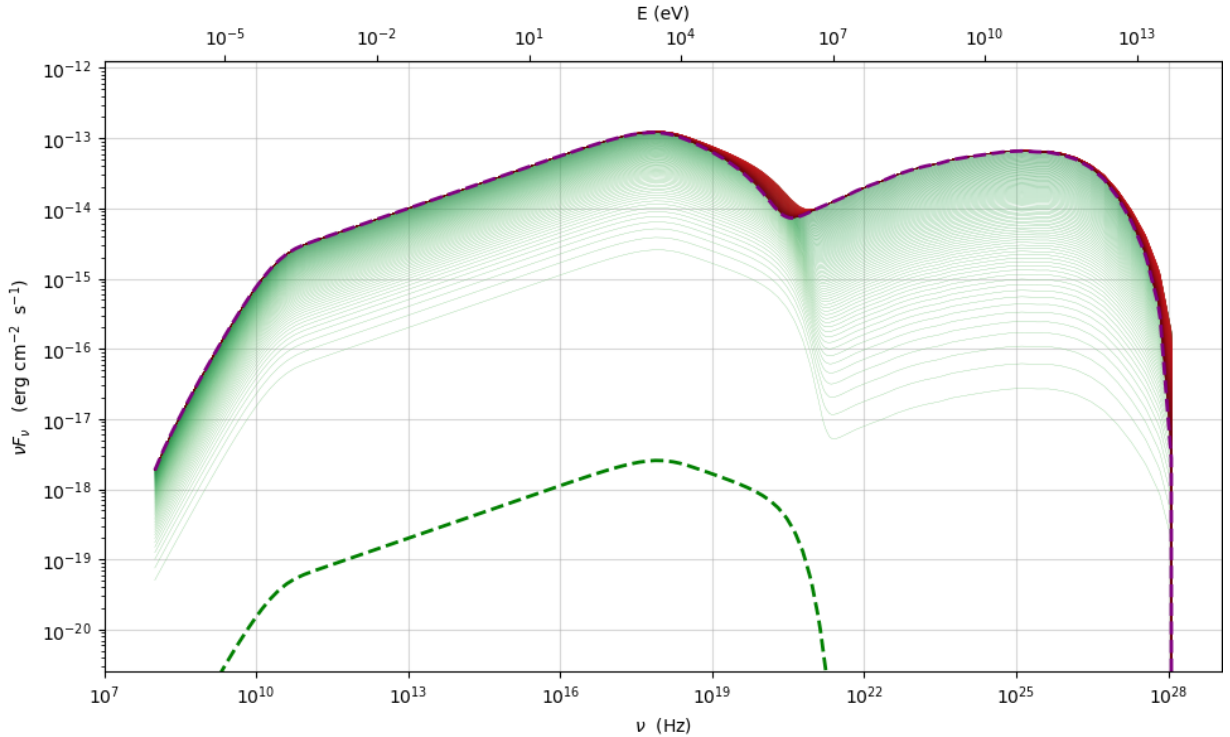


Figure 3. Temporally evolving SED, starting from green dotted lines via red solid lines to purple dotted lines

deceleration radius r_d , where the relativistic swept-up mass equals the initial mass of the plasmoid (e.g., [Dermer & Chiang 1998](#); [Dermer et al. 1999](#)).

Figure 3 presents the temporally evolving SEDs from radio to γ rays from a simulation that provides a fit to the decay of the radio light curve of the decelerating component RK1 observed in MAXI J1348-630 (see below). Notably, the synchrotron emission peaks in the X-ray band, while the SSC spectrum peaks at multi-GeV – TeV γ -ray energies, suggesting that such sources may be detectable by the Fermi Large Area Telescope (LAT) or ground-based Cherenkov Telescope facilities. There is a very small shift in the evolving SED peaks over time, thus predicting no significant time delays between the light curves at different frequencies.

The bottom panel of Figure 4 shows the fit of our model to the angular separation of component RK1 from the central black hole of MAXI J1348-630 as a function of time, as already demonstrated by [Zdziarski et al. \(2023\)](#). The bottom panel of Figure 4 shows the radio light curve of RK1 along with the prediction of our model at a frequency of 1.3 GHz. It illustrates that the decay phase of the radio light curve is well modelled, but the model over-predicts the flux around MJD 58700 – MJD 58730, which could be due to the upper limits from MeerKAT. The maximum 1 – 10 keV X-ray flux predicted by the model, $\sim 10^{-13}$ erg s $^{-1}$ cm $^{-2}$, falls significantly below the observed Swift-XRT flux. This suggests that the X-ray flux is dominated by thermal contributions from the accretion disk and corona, and the jet emission is negligible.

4. SUMMARY AND DISCUSSION

In this paper, we modelled the radio light curve of the low-mass X-ray binary system MAXI J1348-630 during an episode of deceleration of a radio component of the jet of this system. [Zdziarski et al. \(2023\)](#) has shown that a smooth transition between an evacuated cavity around the binary and the ISM, with which the ejected jet component interacts, is capable of reproducing the observed jet deceleration with realistic energy requirements. Motivated by this development, we investigate the radiative signatures of a decelerating plasmoid in the jet of the MAXI J1348-630 microquasar which was first detected in early February 2019, around MJD 58520, corresponding to the beginning of the first outburst phase ([Russell et al. 2019b](#)). This model incorporates the inertia of swept-up material as the plasmoid travels through the surrounding medium, alongside the effects of radiation drag and cooling.

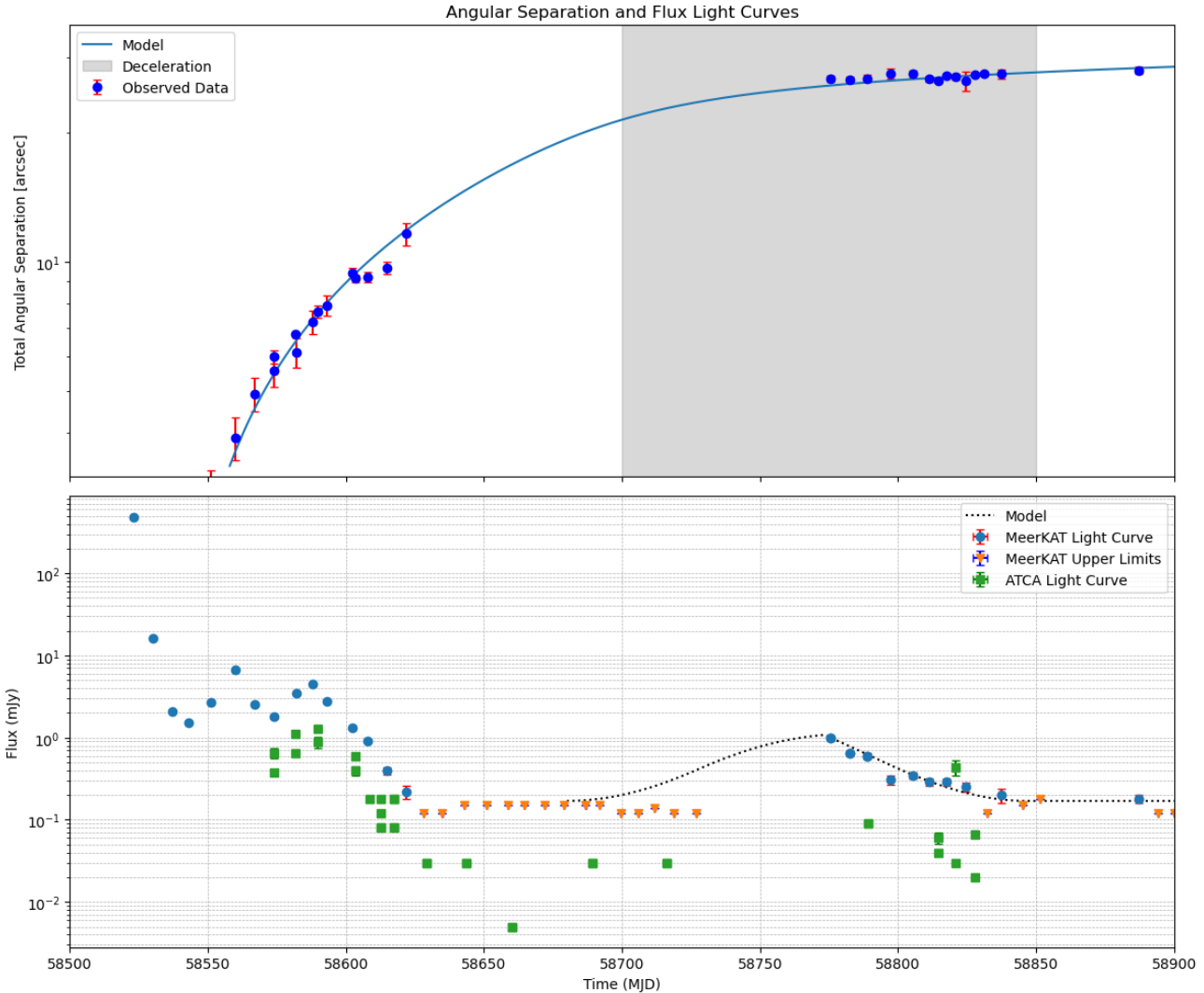


Figure 4. Fit of the decelerating-plasmoid model to the MeerKAT and ATCA radio light curve (data from Carotenuto et al. 2021) the decelerating component RK1 (bottom panel), and of the angular separation of RK1 vs. time (top panel).

Our analysis reveals that, akin to the relativistic blast-wave model used for gamma-ray bursts (GRBs) Chiang & Dermer (1999), the plasmoid undergoes a transition from an initial coasting phase with a nearly constant Lorentz factor to a self-similar deceleration phase. Our model successfully captures the characteristics of the RK1 radio lightcurve that coincided with the observed radio-component deceleration phase, lasting approximately one week. Our analysis predicts no significant time delays between the emissions in different wavelength bands. Our model SEDs (see section 2.3) exhibit a synchrotron peak around X-ray wavelengths, whose flux, however, remains below the dominant thermal contribution from the accretion disk, and an SSC peak at multi-GeV – TeV γ -ray energies, suggesting that such systems may also be detectable by space- or ground-based γ -ray observatories.

A very similar decelerating-blob model had previously been used to obtain a fit to a quasi-exponentially decaying optical lightcurve of the blazar 3C279 (Böttcher & Principe 2009). It offers a promising way to interpret multi-wavelength data of other microquasars in outburst, in which jet ejections and subsequent radio-jet component decelerations are observed. Most notably, XTE J1550–564 showed such an episode around the year 2000. This microquasar was spatially resolved in both radio and X-ray wavelengths, with the radio emission confirmed to be from synchrotron processes, while the origin of the X-rays is still under debate (Corbel et al. 2002b). Proper motion observations using Chandra showed that the eastern jet decelerated between 1998 and 2000, and within about two years, the western jet experienced significant deceleration as well. Also in this case, a smooth transition between an evacuated cavity and the ISM

might substantially reduce the energy requirements of the jet ejection (Zdziarski et al. 2023). The X-ray light curve of the eastern jet had an exponential decay with a e -folding time of $t_{\text{decay}} \sim (338 \pm 14)$ days, which is consistent within uncertainties with the western jet ($t_{\text{decay}} \sim [311 \pm 37]$ days). At the same time, the radio light curve showed a much steeper decay compared to the X-ray light curve (Tomsick et al. 2003b; Migliori et al. 2017). In future work, we will apply our decelerating-blob model to this system to evaluate whether it is able to reproduce the observed kinematics of the radio and X-ray jet components and the corresponding light curves.

5. ACKNOWLEDGMENTS

The authors thank the anonymous referee for constructive criticism and suggestions that have helped to substantially improve the manuscript, and Prof. A. A. Zdziarski for fruitful discussions. The work of MB is supported by the South African Department of Science and Innovation and the National Research Foundation through the South African Gamma-Ray Astronomy Program (SA-GAMMA).

REFERENCES

- Aharonian, F. A., Kelner, S. R., & Prosekin, A. Y. 2010, *PhRvD*, 82, 043002, doi: [10.1103/PhysRevD.82.043002](https://doi.org/10.1103/PhysRevD.82.043002)
- Bambi, C., ed. 2016, *Transient Black Hole Binaries* (Berlin, Heidelberg: Springer Berlin Heidelberg), 61–97, doi: [10.1007/978-3-662-52859-4_2](https://doi.org/10.1007/978-3-662-52859-4_2)
- Belloni, T., ed. 2010, *States and Transitions in Black Hole Binaries* (Berlin, Heidelberg: Springer Berlin Heidelberg), 53–84, doi: [10.1007/978-3-540-76937-8_3](https://doi.org/10.1007/978-3-540-76937-8_3)
- Böttcher, M., & Principe, D. 2009, *ApJ*, 692, 1374, doi: [10.1088/0004-637X/692/2/1374](https://doi.org/10.1088/0004-637X/692/2/1374)
- Carotenuto, F., Tetarenko, A. J., & Corbel, S. 2022, *MNRAS*, 511, 4826, doi: [10.1093/mnras/stac329](https://doi.org/10.1093/mnras/stac329)
- Carotenuto, F., Corbel, S., Tremou, E., et al. 2021, *Monthly Notices of the Royal Astronomical Society*, 504, 444–468, doi: [10.1093/mnras/stab864](https://doi.org/10.1093/mnras/stab864)
- Carotenuto, F., Corbel, S., Tremou, E., et al. 2021, *MNRAS*, 504, 444, doi: [10.1093/mnras/stab864](https://doi.org/10.1093/mnras/stab864)
- Chauhan, J., Miller-Jones, J. C. A., Raja, W., et al. 2020, *Monthly Notices of the Royal Astronomical Society: Letters*, 501, L60, doi: [10.1093/mnrasl/slaa195](https://doi.org/10.1093/mnrasl/slaa195)
- Chen, W.-C., & Podsiadlowski, P. 2019, *The Astrophysical Journal Letters*, 876, L11, doi: [10.3847/2041-8213/ab1b44](https://doi.org/10.3847/2041-8213/ab1b44)
- Chiang, J., & Dermer, C. D. 1999, *The Astrophysical Journal*, 512, 699, doi: [10.1086/306789](https://doi.org/10.1086/306789)
- Chiang, J., & Dermer, C. D. 1999, *ApJ*, 512, 699, doi: [10.1086/306789](https://doi.org/10.1086/306789)
- Corbel, S., Fender, R. P., Tomsick, J. A., Tzioumis, A. K., & Tingay, S. 2004, *ApJ*, 617, 1272, doi: [10.1086/425650](https://doi.org/10.1086/425650)
- Corbel, S., Fender, R. P., Tzioumis, A. K., et al. 2000a, *A&A*, 359, 251, doi: [10.48550/arXiv.astro-ph/0003460](https://doi.org/10.48550/arXiv.astro-ph/0003460)
- . 2000b, *A&A*, 359, 251, doi: [10.48550/arXiv.astro-ph/0003460](https://doi.org/10.48550/arXiv.astro-ph/0003460)
- Corbel, S., Fender, R. P., Tzioumis, A. K., et al. 2002a, *Science*, 298, 196, doi: [10.1126/science.1075857](https://doi.org/10.1126/science.1075857)
- . 2002b, *Science*, 298, 196–199, doi: [10.1126/science.1075857](https://doi.org/10.1126/science.1075857)
- Corbel, S., Nowak, M. A., Fender, R. P., Tzioumis, A. K., & Markoff, S. 2003, *Astronomy & Astrophysics*, 400, 1007–1012, doi: [10.1051/0004-6361:20030090](https://doi.org/10.1051/0004-6361:20030090)
- Denisenko, D., Denisenko, I., Evtushenko, M., et al. 2019, *The Astronomer’s Telegram*, 12430, 1
- Dermer, C. D., & Chiang, J. 1998, *NewA*, 3, 157, doi: [10.1016/S1384-1076\(98\)00004-9](https://doi.org/10.1016/S1384-1076(98)00004-9)
- Dermer, C. D., Chiang, J., & Böttcher, M. 1999, *ApJ*, 513, 656, doi: [10.1086/306871](https://doi.org/10.1086/306871)
- Dermer, C. D., & Menon, G. 2010, *High Energy Radiation from Black Holes: A Summary*. <https://arxiv.org/abs/1001.1760>
- Fender, R. 2003, *Jets from X-ray binaries*. <https://arxiv.org/abs/astro-ph/0303339>
- Fender, R. P. 2001, *Monthly Notices of the Royal Astronomical Society*, 322, 31, doi: [10.1046/j.1365-8711.2001.04080.x](https://doi.org/10.1046/j.1365-8711.2001.04080.x)
- Fender, R. P., Belloni, T. M., & Gallo, E. 2004, *Monthly Notices of the Royal Astronomical Society*, 355, 1105, doi: [10.1111/j.1365-2966.2004.08384.x](https://doi.org/10.1111/j.1365-2966.2004.08384.x)
- Fender, R. P., Garrington, S. T., McKay, D. J., et al. 1999, *Monthly Notices of the Royal Astronomical Society*, 304, 865, doi: [10.1046/j.1365-8711.1999.02364.x](https://doi.org/10.1046/j.1365-8711.1999.02364.x)
- Finke, J. D., Dermer, C. D., & Böttcher, M. 2008, *ApJ*, 686, 181, doi: [10.1086/590900](https://doi.org/10.1086/590900)
- Hannikainen, D. C., Hunstead, R. W., Campbell-Wilson, D., & Sood, R. K. 1998, *MOST Radio Monitoring of GX 339-4*. <https://arxiv.org/abs/astro-ph/9805332>
- Hjellming, R. M., & Rupen, M. P. 1995, *Nature*, 375, 464, doi: [10.1038/375464a0](https://doi.org/10.1038/375464a0)
- Homan, J., Fridriksson, J. K., Jonker, P. G., et al. 2013, *ApJ*, 775, 9, doi: [10.1088/0004-637X/775/1/9](https://doi.org/10.1088/0004-637X/775/1/9)

- Ingram, A. R., & Motta, S. E. 2019, *NewAR*, 85, 101524, doi: [10.1016/j.newar.2020.101524](https://doi.org/10.1016/j.newar.2020.101524)
- Jones, F. C. 1968, *Phys. Rev.*, 167, 1159, doi: [10.1103/PhysRev.167.1159](https://doi.org/10.1103/PhysRev.167.1159)
- Kajava, J. J. E., Motta, S. E., Sanna, A., et al. 2019, *MNRAS*, 488, L18, doi: [10.1093/mnrasl/slz089](https://doi.org/10.1093/mnrasl/slz089)
- Kalemci, E., Dinçer, T., Tomsick, J. A., et al. 2013, *ApJ*, 779, 95, doi: [10.1088/0004-637X/779/2/95](https://doi.org/10.1088/0004-637X/779/2/95)
- Kennea, J. A., & Negoro, H. 2019, *The Astronomer's Telegram*, 12434, 1
- Koljonen, K. I. I., & Russell, D. M. 2019, *The Astrophysical Journal*, 871, 26, doi: [10.3847/1538-4357/aaf38f](https://doi.org/10.3847/1538-4357/aaf38f)
- Körding, E., & Falcke, H. 2005, *Ap&SS*, 300, 211, doi: [10.1007/s10509-005-1193-8](https://doi.org/10.1007/s10509-005-1193-8)
- Lamer, G., Schwobe, A. D., Predehl, P., et al. 2021, *A&A*, 647, A7, doi: [10.1051/0004-6361/202039757](https://doi.org/10.1051/0004-6361/202039757)
- Markoff, S., Nowak, M., Corbel, S., Fender, R., & Falcke, H. 2003, *A&A*, 397, 645, doi: [10.1051/0004-6361:20021497](https://doi.org/10.1051/0004-6361:20021497)
- Markoff, S., Nowak, M., Corbel, S., Fender, R., & Falcke, H. 2003, *Astronomy & Astrophysics*, 397, 645
- Markoff, S., Nowak, M. A., & Wilms, J. 2005, *ApJ*, 635, 1203, doi: [10.1086/497628](https://doi.org/10.1086/497628)
- Matsuoka, M., Kawasaki, K., Ueno, S., et al. 2009, *Publications of the Astronomical Society of Japan*, 61, 999, doi: [10.1093/pasj/61.5.999](https://doi.org/10.1093/pasj/61.5.999)
- Migliori, G., Corbel, S., Tomsick, J. A., et al. 2017, *Monthly Notices of the Royal Astronomical Society*, 472, 141, doi: [10.1093/mnras/stx1864](https://doi.org/10.1093/mnras/stx1864)
- Miller-Jones, J. C. A., Sivakoff, G. R., Altamirano, D., et al. 2012, *MNRAS*, 421, 468, doi: [10.1111/j.1365-2966.2011.20326.x](https://doi.org/10.1111/j.1365-2966.2011.20326.x)
- Mirabel, I. F., & Rodríguez, L. F. 1994, *Nature*, 371, 46, doi: [10.1038/371046a0](https://doi.org/10.1038/371046a0)
- Nesci, R., & Fionchi, M. 2019, *The Astronomer's Telegram*, 12448, 1
- Poutanen, J., Veledina, A., & Revnivtsev, M. G. 2014, *MNRAS*, 445, 3987, doi: [10.1093/mnras/stu1989](https://doi.org/10.1093/mnras/stu1989)
- Remillard, R. A., & McClintock, J. E. 2006, *Annual Review of Astronomy and Astrophysics*, 44, 49, doi: <https://doi.org/10.1146/annurev.astro.44.051905.092532>
- Ribo, M., Dhawan, V., & Mirabel, I. F. 2004, *The asymmetric compact jet of GRS 1915+105*. <https://arxiv.org/abs/astro-ph/0412657>
- Russell, D. M., Bramich, D. M., Lewis, F., et al. 2019a, *Astronomische Nachrichten*, 340, 278
- . 2019b, *Astronomische Nachrichten*, 340, 278–283, doi: [10.1002/asna.201913610](https://doi.org/10.1002/asna.201913610)
- Sanna, A., Bult, P., Ng, M., et al. 2022, *Monthly Notices of the Royal Astronomical Society: Letters*, 516, L76, doi: [10.1093/mnrasl/slac093](https://doi.org/10.1093/mnrasl/slac093)
- Steiner, J. F., McClintock, J. E., Remillard, R. A., et al. 2010, *ApJL*, 718, L117, doi: [10.1088/2041-8205/718/2/L117](https://doi.org/10.1088/2041-8205/718/2/L117)
- Tominaga, M., Nakahira, S., Shidatsu, M., et al. 2020, *ApJL*, 899, L20, doi: [10.3847/2041-8213/abaaaa](https://doi.org/10.3847/2041-8213/abaaaa)
- Tomsick, J. A., Corbel, S., Fender, R., et al. 2003a, *The Astrophysical Journal*, 582, 933, doi: [10.1086/344703](https://doi.org/10.1086/344703)
- . 2003b, *The Astrophysical Journal*, 582, 933, doi: [10.1086/344703](https://doi.org/10.1086/344703)
- Tramacere, A. 2020, *JetSeT: Numerical modeling and SED fitting tool for relativistic jets*, *Astrophysics Source Code Library*, record ascl:2009.001
- Tramacere, A., Giommi, P., Perri, M., Verrecchia, F., & Tosti, G. 2009, *A&A*, 501, 879, doi: [10.1051/0004-6361/200810865](https://doi.org/10.1051/0004-6361/200810865)
- Tramacere, A., Massaro, E., & Taylor, A. M. 2011, *ApJ*, 739, 66, doi: [10.1088/0004-637X/739/2/66](https://doi.org/10.1088/0004-637X/739/2/66)
- Yatabe, F., Negoro, H., Nakajima, M., et al. 2019, *The Astronomer's Telegram*, 12425, 1
- Zdziarski, A. A., & Gierliński, M. 2004, *Progress of Theoretical Physics Supplement*, 155, 99, doi: [10.1143/PTPS.155.99](https://doi.org/10.1143/PTPS.155.99)
- Zdziarski, A. A., Sikora, M., Szanecki, M., & Böttcher, M. 2023, *The Astrophysical Journal Letters*, 947, L32, doi: [10.3847/2041-8213/accb5a](https://doi.org/10.3847/2041-8213/accb5a)